The Influence of Water Absorption on Unidirectional and 2D Woven CFRP Composites and their Mechanical Performance

Faisel Almudaihesh, Karen Holford, Rhys Pullin, Mark Eaton.

Abstract

This paper discusses a key parameter 'fibre architecture' that is believed to play a major part in the performance of CFRP composites when subjected to water absorption. Unidirectional, plain, and twill weave CFRP specimens were immersed in water at 70°C for 40 days. The condition of the matrix was examined using a Scanning Electron Microscope (SEM). The mechanical properties dominated by the condition of the matrix and interfacial regions such as compression, shear, and impact resistance were assessed for un-aged and aged specimens. A reduction in strength was observed for all aged specimens. However, the observed reduction in strength varies depending on both the fibre architecture used and the specific load case. The largest effect on properties was observed in unidirectional materials, which leads to the recommendation that less conservative safety factors should be used for woven fibre architectures.

1. Introduction

The use of CFRP composites are significantly increasing in the aerospace, automotive and marine industries, particularly in safety critical primary structures, due to their excellent fatigue and corrosion resistance properties as well as their high strength-to-weight and stiffness-to-weight ratios compared with metallic materials [1]. However, their inherent reactions to environmental and structural impacts is still a significant concern in real life applications [2].

Polymers are known to degrade in moist environments by reacting with water in a hydrolysis process which effects their mechanical performance [3]. The influence of water ingress on fibrous-polymer composites varies based on temperatures and water type, such as sea water or demineralised water [4]. Higher temperatures are known to have more influence in accelerating the moisture absorption and degradation process in polymers [5,6]. This can also lead to significant changes in the overall intrinsic structural performance and failure mechanisms of CFRP [7–11].

In the case of thermoset polymers, it has been known for some time that the matrix and fibre-matrix interface dominated properties are most affected by moisture adsorption Selzer and Friedrich [12] showed that for unidirectional carbon fibre reinforced epoxies, transverse, compression and interlaminar fracture properties reduced significantly following moisture absorption, whereas no discernible change was observed in fibre direction tensile properties. This corresponds to the accepted mechanisms of moisture absorption in CFRP laminates, which starts with free water molecules at the surface travelling through surface micro-cracks and voids (**Fig. 1** (stage I-III)). This leads to
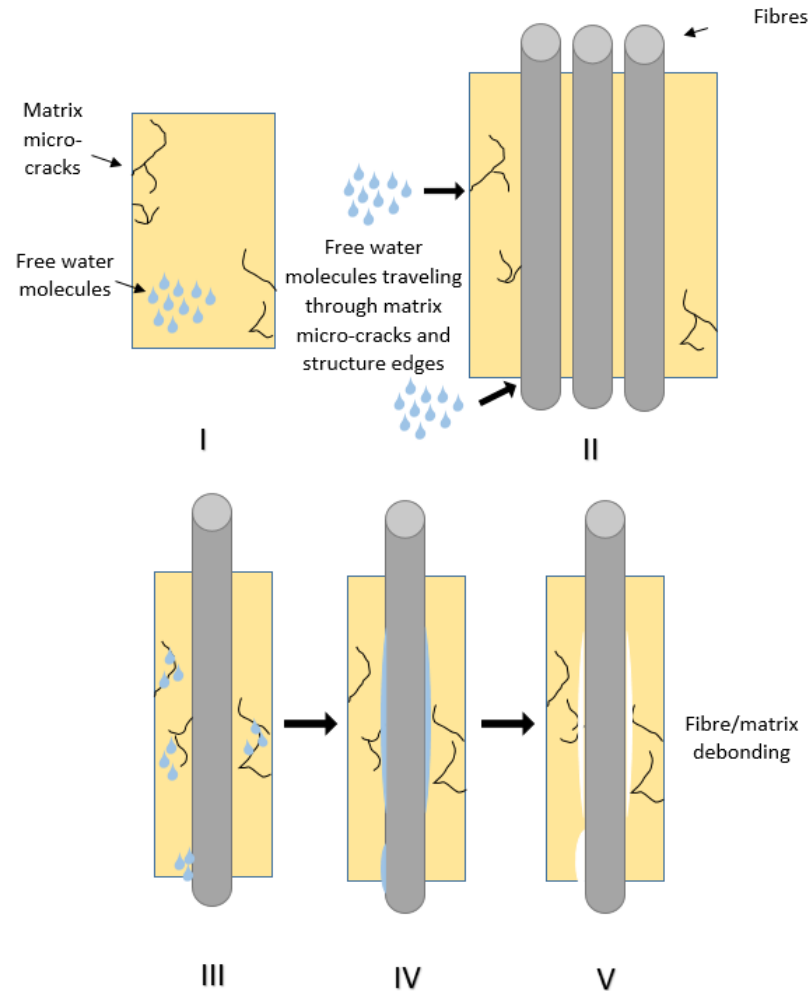
hydrolysis, which has a plasticizing effect leading to a reduction in properties. When water molecules reach the fibre-matrix interface the resultant degradation leads to the reduction of stress transfer [9,13] (**Fig. 1** (stages IV)). Ultimately debonding can occur as the polymer continues to degrade [14–16] (**Fig. 1** (stage V)). This process is dependent on time, temperature, fibre architecture, layup, fibre volume fraction, void content, polymer type, fibre sizing or surface treatment, water type, and contact area [4,9,15,17–19]. However, the extent to which each of these factors affects the final properties of a composite is not clear. The variety of constituent materials, hydrothermal conditioning and properties measured in the current literature makes it challenging to draw consistent conclusions.

Most researchers have studied the influence of moisture absorption on the mechanical properties of CFRP materials with unidirectional fibre architectures. A general trend for reductions in matrix/interface dominated properties is observed. A consistent and significant loss of interlaminar strength is seen by researchers with reductions in short beam shear strength of 26% [11], 22-25% depending on sizing [9] and 29% [20] observed in $[0]_n$ carbon fibre-epoxy laminates. A 15% reduction in mode II fracture toughness was also observed by Selzer and Friedrich [12] during end-notched flexural tests of $[0]_n$ laminates. Significant losses in compression properties are also reported in the case of $[0]_n$ carbon fibre-epoxy laminates with reductions of 26-33% depending on matrix system used [12] and 19% [20] observed. A loss in compression strength was also observed in quasi-isotropic layups with UD fibre architectures, with reductions varying from 10-30% depending on layup used [21]. This was shown to increase further, up to 50%, in the presence of through thickness stitching.

However, in cases where differing fibre architectures are considered, the same reductions in properties are not always seen. Kawai et al [22] considered hydrothermal effects on plain weave fibre architectures with quasi-isotropic layups and showed that the compressive strengths reduced by only 6%. Saito and Kimpara [10] considered the hydrothermal effects on compression after impact (CAI) strength and post impact fatigue (PIF) (R=-1) performance of a plain weave (T300-3K) fibre architecture and a multi-axial knitted fabrics (T700-12k, consisting of UD layers with through thickness stitching). Moisture absorption had little influence on the CAI strength for both materials and on the PIF performance of the woven material. Significant influence; however, was observed in the PIF performance of the multi-axial knitted fabric reducing cycles to failure by 1-2 orders of magnitude. This suggests that the fibre architecture can have a significant influence on the residual strength of materials exposed to moist environments and that observed reductions, and therefore appropriate safety factors, can vary for each material and each property. This has important implications in the design of composite components and structures, particularly where minimising weight is a priority.

This study aims at further understanding the role of fibre architecture in the water absorption mechanism and somewhat more importantly the consequential reduction in strength that corresponds to each architecture. Materials with three different fibre architectures are investigated. The fibre type and resin system were kept the same for all samples, in order to isolate the influence of fibre architecture. Properties with a dependency on matrix and interface properties are investigated, in particular

compression, short beam shear, and impact resistance are considered. Clear differences are identified and the mechanisms are discussed.

Fig. 1. Water ingress mechanism in fibrous reinforced polymers composites.

2. Materials

Three versions of CFRP prepreg were used in this work. All were manufactured by SK Chemicals using Skyflex K51 Epoxy resin to eliminate the influence of polymer type. The specification of each prepreg variant used were: 15k Unidirectional (UD), Pyrofil TR50S high strength carbon fibre 200gsm with 33% resin content; 3k plain weave, Pyrofil TR30S

high strength carbon fibre 198gsm with 40% resin content; and 2x2 3k twill weave, Pyrofil TR30S high strength carbon fibre 198gsm with 40% resin content. Fibres sizing levels were 1.0% and 1.2% for Pyrofil TR50S and Pyrofil TR30S, respectively. All carbon fibres featured the same filament diameter of 7um, the same yield of (1000 mg/m for 15K and 200 mg/m for 3K), and the same tensile modulus of 235GPa. The tensile strength, elongation at break, and density were slightly different with 4.90GPa, 2.1%, and 1.82g/cm^3 for Pyrofil TR50S, respectively, and 4.12GPa, 1.8%, and 1.79 g/cm^3, for Pyrofil TR30S, respectively. All materials were cured with the same cure cycle, as recommended by the material supplier, using an autoclave under two dwells, 30 minutes at 80°C temperature and 5 bar pressure followed by 60 minutes at 125°C temperature and 5 bar pressure. Large panels were manufactured with the required stacking sequences and cut into the desired specimen dimensions. All panels were inspected by c-scaning (using MIDAS NDT Systems Ltd with pulse-receive mode using a 10MHz probe) to ensure manufacturing quality. The constituent and void contents were obtained for all specimens by matrix digestion for a minimum of three specimens per category in accordance with ASTM D3171 method 1 procedure A [23]. This was carried out by using 60ml nitric acid for each specimen at 80°C for six hours. The carbon fibres were then filtered into pre-weighed sintered glass filters under a vacuum of higher than 17 kPa. The carbon fibres were cleaned with water at least three times and a final acetone wash followed by one hour oven drying at 100°C. They were then left to cool to room temperature. The weight was then recorded to the nearest 0.0001g using a Sartorius LA310S analytical balance.

3. Experimental Methods

3.1 Water Absorption

Water absorption testing was carried out using non-ambient moisture conditioning in a water immersion tank at a prescribed constant temperature of 70°C for a fixed-time period of 40 days, in accordance with ASTM D5229 (conditioning method of procedure code BWFF) [24]. Still natural spring water was used with typical contents values of 48.5mg/l calcium, 5.2mg/l magnesium, 14.0mg/l sodium, 0.8mg/l potassium, 148.0mg/l bicarbonate, 10.7mg/l chloride, 27.6mg/l sulphate, and 4.0mg/l nitrate. An unstirred digital bath (NE2-28D) supplied by Clifton with a sensitivity of ±0.2°C and uniformity of ±0.1°C was used and specimens were placed in the bath once steady-state temperature was reached. For weighing records, specimens were individually removed from the water bath, left in a sealed bag until it reached an acceptable temperature for laboratory handling (room temperature). The specimens are then removed from bag, surface moisture wiped, mass change measured using analytical balances with accuracies of 0.0001g (Sartorius LA310S analytical balance) for specimens ≥5g but <50g and 0.001g (Adam Nimbus NBL 623i analytical balance) for specimens ≥50g. Samples were then returned to the water bath. The specimen water content was determined as a percentage change using Equation (1)[24]:

$$Mass\ percentage\ change, \% \ = \ \left(\frac{W_i - W_o}{W_o}\right) \times 100 \qquad (1)$$
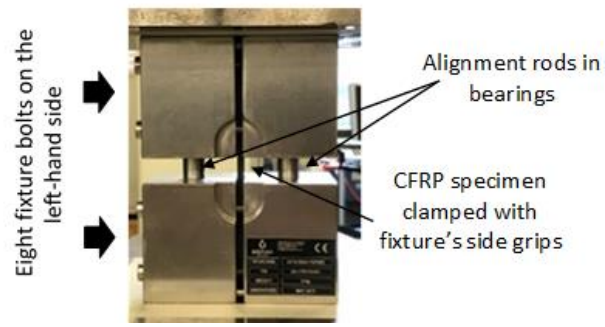
Where:

W_i = weight of the specimen at each point of the weight recorded during the experiment;

W_o = initial weight of the specimen before any contact with water.
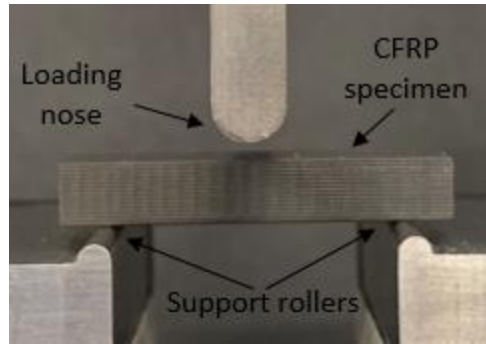
3.2 Compressive Strength

A Combined Loading Compression (CLC) test illustrated in **Fig. 2** was used to determine the laminate compressive strength for un-aged and water-immersed CFRP specimens in accordance with ASTM D 6641 [25]. Ten specimens were prepared for each fibre architecture (five un-aged and five aged). Specimens were 140mm (±0.3mm) long by 13mm wide and a gauge length of 13mm was used. Samples consisted of sixteen plies with a layup of $[0/90]_{4S}$ and $[(0/90)]_{16}$ for UD and woven (plain and twill) materials producing thicknesses of 3.1mm and 3.5mm, respectively. These stacking sequences create an identical distribution of fibre directions between the unidirectional and woven specimens for comparison purposes. A 1 mm thick aluminium caul plate covered with nylon was used inside the vacuum bag to ensure both surfaces of the samples were smooth and suitable for the CLC fixture grips. The matrix volume fraction and void content for compression specimens were obtained from three 20mm by 13mm specimens cut from the manufactured panels. An Avery-Denison loading machine with 600kN load cell with fixed loading platens was used to apply load to the CLC fixture at a rate of 1.3mm/min. The CLC fixture screws were tightened with a torque of 3.5N-m as recommended in the standard.

Fig. 2. CLC test configuration.

3.3 Interlaminar Strength

The interlaminar strength was investigated by employing the short-beam strength test method by using a three-point bend (3PB) fixture shown in **Fig. 3**. The diameter of support rollers is 3mm, the diameter of the loading nose is 6mm and the span is 24mm. A Zwick Roell Z050 load machine, with 50kN load cell, was used to apply load at a crosshead rate of 1mm/min in accordance with ASTM D2344 [26]. Ten specimens with dimensions 36mm by 12mm were prepared for each fibre architecture (five un-aged and five aged). Samples consisted of thirty plies with a layup of $[0/90]_{15}$ and $[(0/90)]_{30}$ for UD and woven (plain and twill) materials with thicknesses of 5.8mm and 6.4mm, respectively. Due to the sample thickness a debulking operation (5 minutes vacuum) was undertaken after each five plies [27]. The fibre volume fractions and void content for these specimens were obtained from three 12mm by 10mm specimens cut from the manufactured panels.
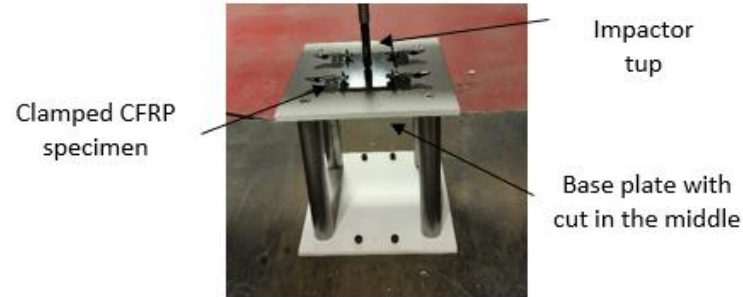
Fig. 3. 3PB test configuration.

3.4 Impact Resistance

The Impact Damage Resistance (IDR) was assessed in accordance with ASTM D 7136 [28] with the fixture shown in **Fig. 4**. Specimens were prepared with dimensions of 150mm (±0.25mm) by 100mm (±0.25mm) and layups of $[45/0/-45/90]_{3s}$ and $[(45/-45)/(0/90)]_{6s}$ for unidirectional and woven (plain and twill) materials, giving thicknesses of 4.5mm and 4.8mm, respectively. A perforated release film and double layer of breather fabric were used in order to facilitate air/gas removal from these larger panels. The fibre volume fractions and void content were obtained from an average of three 20mm by 15mm specimens cut from the as manufactured panels. To investigate the influence of impact damage on water uptake 10 specimens of each fibre architecture were impacted prior to aging. Five were impacted with an energy of 20J, and 5 with an energy of 70J to represent Barely Visible Impact Damage (BVID) and Visible Impact Damage (VID), respectively. A further five specimens were left undamaged for comparison. The undamaged specimens were subsequently impacted with 70J following aging, in order to investigate the influence of moisture absorption on impact resistance. Impact testing

was undertaken using an Instron 9250-HV drop tower, with a 16mm (±0.1) diameter hemispherical impact tup and a mass of 5.5kg.

Fig. 4. IDR test configuration.

4. Results and Discussions

4.1 Constituent Contents

Table 1 presents the constituent contents for all specimens. The matrix volume fraction is similar for the CLC and 3PB samples of the same material and as would be expected the woven architectures result in a higher matrix content. The IDR samples exhibit comparatively lower matrix volume fractions, due to the perforated release film used in manufacture, but a trend for higher matrix content in woven architectures is still present. Void contents are seen to be low and, with the exception of the UD IDR sample, are all below 1%, which is in line with aerospace standards [29].

Table 1

Constituent contents.

Specimen Type	V_m (%)			V_{air} (%)		
	UD	Plain	Twill	UD	Plain	Twill
CLC	41.6	47.47	48.92	0.75	0.38	0.14
3PB	40.55	48.49	47.58	0.86	0.72	0.48
IDR	39.76	43.69	43.91	1.12	0.82	0.83

4.2 Water Absorption

For CLC and 3PB specimens, the mass change was measured at the start and end of the water experiment and the results are presented in **Fig. 5**. Error bars represent the maximum and minimum values observed from five specimens. It is noted that the 3PB specimens had an initial, un-aged, weight that varied between 3.5 to 4g, which is below the minimum of 5g recommended in ASTM D5229 [24]. The total percentage mass gains for all specimens are presented in **Table 2**, along with the mass gain as a percentage of the matrix only (using data from **Table 1**) and the surface area to volume ratios.

Fig. 5. Average weight percentage increase in CLC and 3PB specimens.

The total mass gains, for the composite, vary quite significantly between sample types and smaller variations occur between fibre architectures within each sample type. These variations are seen to correlate strongly to the surface area to volume ratio of the samples. Plotting the surface area to volume ratio against total mass gain shows a linear correlation with an R^2 value of 0.95 (supplementary information **Fig. S1**) suggesting that
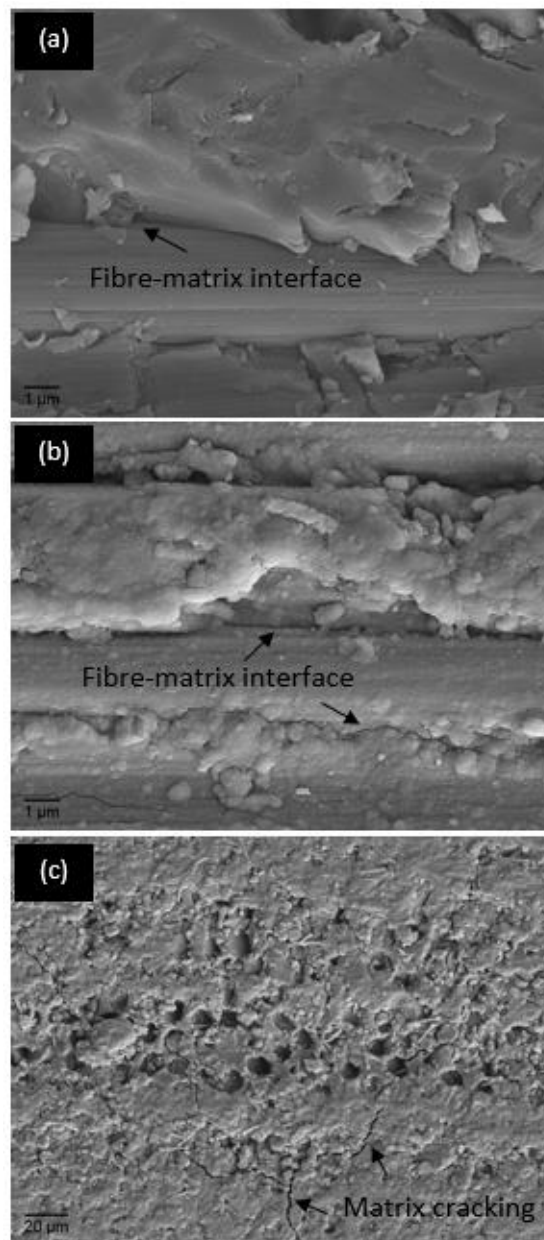
these variations result from geometry and not material differences. When considering the mass gain as a percentage of the matrix only the same correlation is observed, however, mass gain is greater for a given surface area to volume ratio in the UD samples (supplementary information **Fig. S2**). This suggests that diffusion rates are greater in the UD material and this can be correlated to the linearity of the fibre paths, providing direct water ingress into the structure along the fibre matrix interface (**Fig. 1** Stage IV) [30]. In woven architectures, the weave patterns are believed to act as barriers, providing a longer path for moisture ingress along the fibre-matrix interface. This effect may be exacerbated by the sizing levels, as the UD fibre have a lower sizing level and therefore may allow easier degradation of the fibre matrix interface. Evidence of the degradation of the fibre-matrix interface is seen in the Scanning Electron Microscope (SEM) images in **Fig. 6** (b-c) for the aged UD material.

Table 2

Summary of water absorption results.

Specimen Type	Total surface/volume ratio			Matrix weight increase (%)*			Composites weight increase (%)		
	UD	Plain	Twill	UD	Plain	Twill	UD	Plain	Twill
CLC	0.82	0.73	0.74	4.066	3.217	3.314	1.316	1.217	1.294
3PB	0.57	0.51	0.53	3.186	2.380	2.599	0.998	0.938	0.989
IDR (0J)	0.47	0.44	0.45	2.783	2.134	2.084	0.854	0.737	0.724
IDR (20J)	0.47	0.44	0.45	2.903	2.2	2.167	0.892	0.760	0.753
IDR (70J)	0.47	0.44	0.45	3.243	3.170	2.899	0.996	1.095	1.011

* The mass change due to moisture absorption as a function of matrix content was achieved by multiplying the resin weight fraction of each specimen by its overall weight and calculating the mass change assuming no moisture effects were observed from the carbon fibres.

Fig. 6. SEM micrographs of UD surface: (a) interface of un-aged UD specimen; (b) interface of aged UD specimen; (c) matrix cracking in aged UD specimen.
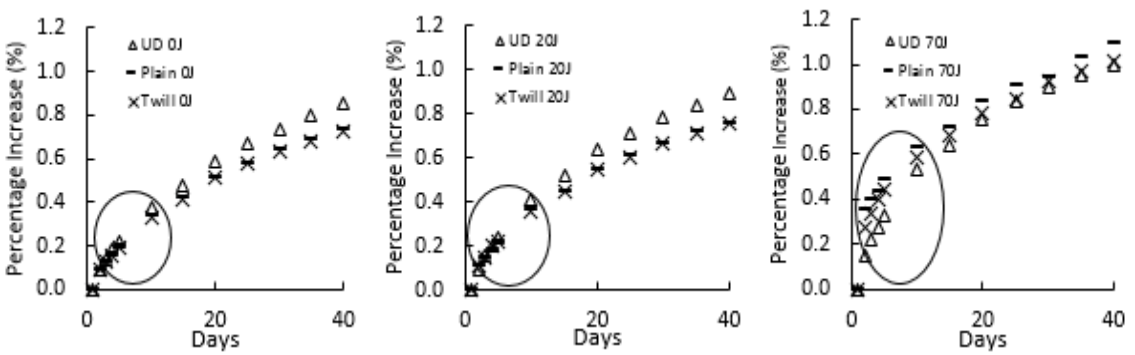
This is in line with the proposed theory in **Fig. 1**. where the water penetration mechanism is initially breaking through the matrix increasing the crack density and subsequently detaching the fibre-matrix interface. A similar response is seen for the plain and twill woven architectures as shown by the SEM images in supplementary

information **Fig. S3-S10**. Furthermore, the mineral content attained in the type of water used are believed to have caused a deposition of salts on the surface, which was clearly observed from matrix condition in aged specimens compared with their dry equivalents.
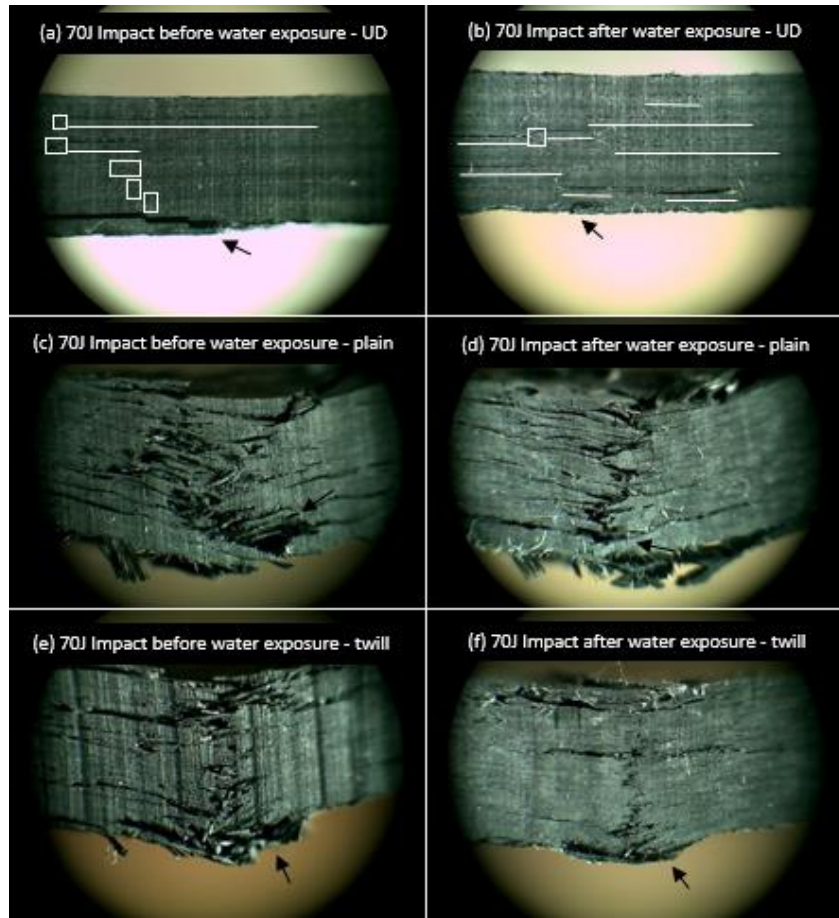
In the case of the IDR specimens, additional mass change measurements were made throughout the water absorption experiment in order to study the influence of impact damage level on moisture uptake. The curves of mass gain versus time are shown in **Fig. 7** for each damage level and the total mass gains are presented in **Table 2**. The total percentage mass gain in the undamaged IDR sample is lower, compared with the CLC and the 3PB samples, due to their lower surface area to volume ratio (**Table 2**). Differences in mass gain between the IDR sample types also correlate to the surface area to volume ratio. This correlation remains at the 20J (BVID) damage level (with only marginal increases in total mass gain observed, compared with undamaged samples) but not at the 70J (VID) damage level due to the effects of the increasing damage volume. The greatest increase in mass for the damage samples, shown in **Fig. 7,** occurs in the earlier stages of the moisture absorption experiment up to the 'knee' in the curve at approximately 10 days. The gradients after this point are very similar for all specimens, suggesting that moisture ingress in to the free volume in the damage region is driving this increase. The larger mass gain seen in the 70J damage level samples results from a higher damage volume but also a larger amount of surface cracking allowing rapid ingress to the damage volume. This results in the woven architectures now absorbing more water than the UD material. **Fig. 8** shows cross-sectional micrographs of the damage induced by 70J impacts and demonstrates how more significant through thickness damage links to surface cracks in the woven architectures, explaining why the

mass gain increases above that of the UD samples at this damage level. Cross-sectional

micrographs of the damage induced by 20J impacts can be seen in the supplementary

information **Fig. S11** for comparison.

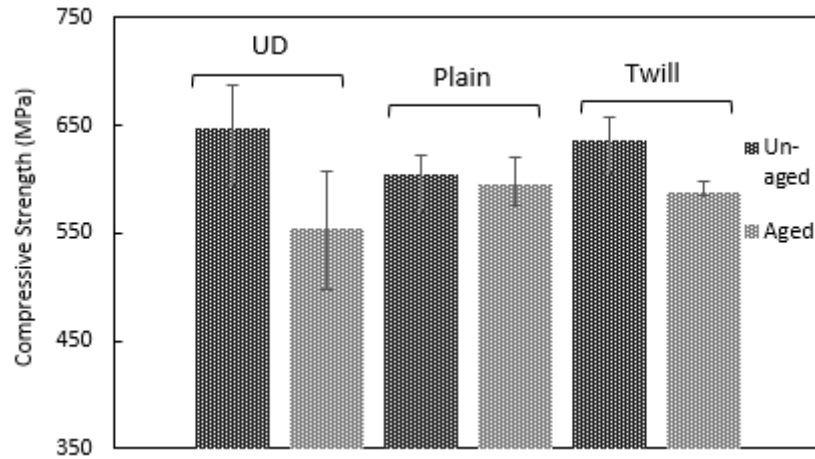**Fig. 7**. Percentage of weight increase in IDR specimens

Fig. 8. IDR specimens after failure; images are showing a length of 12mm (±0.25mm) of the middle section of the specimen's impact damage area.

4.3 Mechanical Properties

The results of compressive strength achieved by CLC testing are presented in **Fig. 9**. In the case of the un-aged samples the UD fibre architecture exhibits the highest strength, followed by the twill weave and then the plain weave. As compressive failures are initiated by microbuckling of the fibres it makes sense that the strength would reduce in this way, as the fibres are misaligned in the woven architectures with the plain weave having the greatest misalignment along with the fact that Pyrofil TR50S featured slightly

higher tensile strength compared with Pyrofil TR30S. The moisture absorption process in the aged specimens induces plasticisation of the matrix, along with microcracking, which reduces the support of the fibres [12,31–33]. Hence, a reduction in strength is observed in all aged specimens, however, the magnitude of the reduction varies greatly. The woven architectures exhibit much smaller reductions in strength, because the distorted fibres already have a propensity to buckle, particularly in the case of the plain weave where a negligible reduction (1.34%) is seen. The reduction increases to 7.5% for the twill weave where the straighter fibres rely more on the support of the matrix to resist buckling. The largest reduction is seen in the UD material at 14.6% where the straight fibres require good support of the matrix to carry higher stresses and therefore fail at much lower loads in the aged samples [34–36]. The occurrence of microbuckling in UD fibres is usually preceded by either local matrix yielding or debonding of the fibre-matrix interface [37]. This correlates to the greater mass gain as a percentage of matrix content observed in the UD samples (**Table 2**), which suggests either greater plasticisation or interface degradation has occurred and would therefore promote an earlier failure in these samples. The lower level of fibre sizing in the UD samples could also exacerbate this behaviour. Importantly the reduction in strength of the aged UD material is significantly large that it becomes weaker than both of the woven fibre architectures in an aged condition. This has great significance when considering material selection and safety factors for carbon fibre composites operating in moist environments.

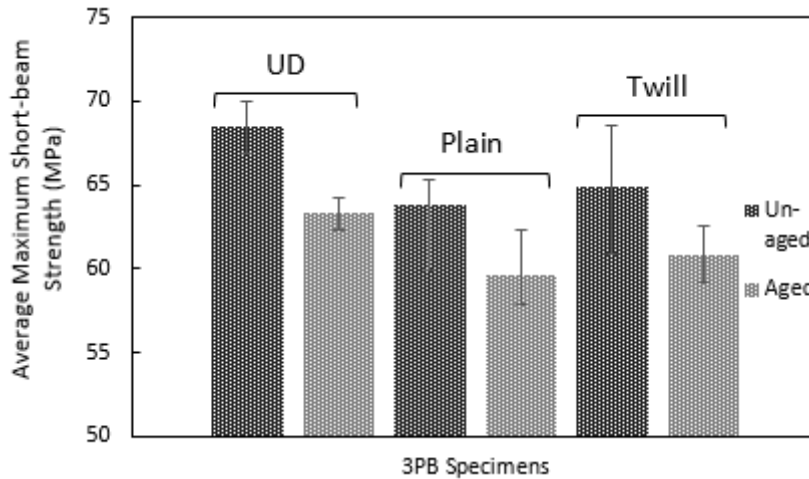**Fig. 9.** Compressive strength for un-aged and aged CFRP specimens

This corresponds to the observed failure modes in **Fig. 10** where the relative ease of microbuckling induced failure in the plain weave samples leads to a through thickness crack in the un-aged samples. Conversely significant brooming is seen in the failure for the un-aged UD samples, whereas the twill weave samples exhibit both brooming and through thickness cracking. After aging all samples exhibited significantly less interlaminar cracking / brooming, which corresponds to the increased ductility and toughness of the matrix [38]. The aged UD samples exhibited mostly through thickness cracking with a significant reduction in the presence of any brooming, due to the premature microbuckling of less well supported fibres. The aged plain weave samples exhibited the same through thickness cracking mechanism but with less localised interlaminar cracking observed. The aged twill weave samples exhibited more through thickness cracking with much less brooming and interlaminar fracture observed. It is noted that all failure modes observed were deemed acceptable in accordance with those reported in ASTM D 6641 [25].

Fig. 10. CLC specimens after failure; images are showing a length of 12mm (±0.25) of the middle section of the specimen's gauge area.

The short beam shear strength of the materials are presented in **Fig. 11** where the woven architectures exhibit the highest unaged strengths, with the through thickness shear stresses that develop from alternating 0,90 layers leading to failure initiation at a lower stress in the UD samples. This type of interlaminar shear failure is dominated by matrix properties and the fibre-matrix interface strength and hence a corresponding
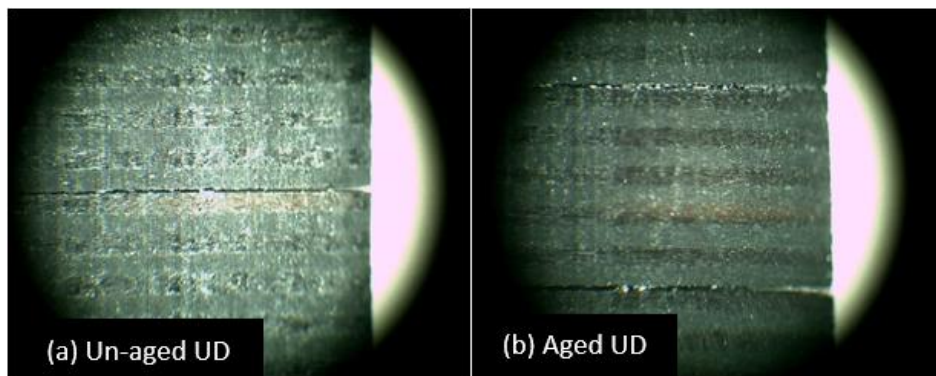
reduction in strength is seen in all cases for the aged samples. This results from the degradation of the fibre-matrix interface (seen in **Fig. 6**) allowing the easy initiation and propagation of interlaminar shear cracks. The greatest reduction is again seen for the UD material with a 7.8 % reduction compared to 6.7 % and 6.5% reductions for the plain and twill weaves, respectively. This again correlates to the higher moisture uptake, as a percentage of the matrix, seen in the UD material. It particularly highlights a greater degradation of the fibre-matrix interface in this material which may also be influenced by the lower levels of sizing in the UD material.

Fig. 11. Short-beam properties for un-aged and aged CFRP specimens.

A single delamination along the longitudinal axis and near to the mid-plane was observed for all un-aged UD specimens, with more than one delamination observed in all aged UD specimens as seen in **Fig. 12**. It is believed that the degradation promoted by water exposure in UD specimens has increased the crack density in the interlaminar regions particularly in the fibre-matrix interface region observed from the SEM micrographs which in turn favoured several longitudinal cracks as reported by Barbosa Et al [5]. Similar behaviour was observed for woven specimens with a single longitudinal

crack near the mid-plane in the middle section of the specimen in the un-aged specimens, with more than one longitudinal crack observed in all aged woven specimen and can be seen in the supplementary information **Fig. S12-S15**. The longitudinal cracks; however, in woven specimens did not grow into delamination along the longitudinal axis due to the weave structure that eliminated the cracks to grow into delaminations as observed in the UD specimens.

Fig. 12. Failure modes of 3PB UD specimens.

The influence of moisture absorption on impact damage resistance was investigated by comparison of 70J impacts prior to aging and after aging. **Table 3** shows the diameter of induced damage determined by ultrasonic C-scanning in accordance with ASTM D 7136 [28]. Very little change in damage size is observed for both woven fibre architectures, whereas an increase of 11.5% is seen in the UD samples. The damage size in woven materials is limited by the extent of longitudinal splitting that can occur in each ply. The woven structure means that long splits cannot form and subsequently grow in to delaminations, as they do in UD materials. The cross-sectional micrographs in **Fig. 8** show that there is a change in the damage formation in woven materials with fewer interlaminar cracks observed (corresponding to increased matrix ductility and

toughness) and a single large through thickness crack. The reduction in interface strength in the aged UD material leads to a greater number of interlaminar cracks (delaminations) that spread over a larger area. This is in agreement with failure observed in the aged 3PB UD specimens, demonstrating several longitudinal cracks **Fig. 12**. This further suggests that the woven fibre architectures perform better in an aged condition compared with UD fibres.

Table 3

The average extent of internal damage diameter from maximum distance across the damage (average of 5 specimens).

Impact Type	Internal Damage Diameter (mm) (±0.2)		
	UD	Plain	Twill
20J before water immersion	43.72	24.86	26.24
70J before water immersion	96.96	36.45	34.11
70J after water immersion	108.12	36.27	33.70

5. Conclusions

The role of fibre architecture in the loss of mechanical properties by environmental degradation has been investigated for carbon fibre reinforced epoxy materials. Whilst the degradation process only takes place in the matrix, the fibre architecture has been shown to influences how failure occurs and how the failure mechanisms change when the matrix degrades. This affects the residual strength of the materials and is therefore a key parameter for materials performance in moist environments. More significant reductions in the mechanical properties were observed in UD specimens after aging, when compared with woven equivalents. In particular, the loss of compressive strength in aged UD materials is large enough (14.6% compared with 1.3% and 7.5% for the plain and twill architectures, respectively) that its residual

strength was below that of both woven architectures. This coupled with the lower un-

aged interlaminar strength that suffered a larger percentage reduction of 7.8 %

compared with 6.7%, and 6.5% for plain and twill architectures, respectively, means the

UD architecture also demonstrated less resistance to impact damage.

It is feasible then, that under exposure to moist environments, a material with a woven

fibre architecture might outperform a UD material, which is often considered superior.

This highlights that a better understanding of the role of fibre architecture in the failure

of aged CFRP materials is needed and that care should be taken in selecting materials

and applying safety factors for such applications. Designers should also bear in mind that

the optimum material/design for an application may not be the most intuitive choice

based on un-aged properties.

References

[1]   Takeda SI, Tsukada T, Sugimoto S, Iwahori Y. Monitoring of water absorption in CFRP laminates using embedded fiber Bragg grating sensors. Compos Part A Appl Sci Manuf 2014;61:163–71. doi:10.1016/j.compositesa.2014.02.018.

[2]   Baley C, Davies P, Grohens Y, Dolto G. Application of Interlaminar Tests to Marine Composites. A Literature Review. Appl Compos Mater 2004;11:99–126. doi:10.1023/B:ACMA.0000012902.93986.bf.

[3]   Masoumi S, Valipour H. Effects of moisture exposure on the crosslinked epoxy system: An atomistic study. Model Simul Mater Sci Eng 2016;24:035011.

[4]   Davies P, Le Gac P-Y, Le Gall M. Influence of Sea Water Aging on the Mechanical Behaviour of Acrylic Matrix Composites. Appl Compos Mater 2017;24:97–111. doi:10.1007/s10443-016-9516-1.

[5]   Cysne Barbosa AP, Ana AP, S.S. Guerra E, K. Arakaki F, Tosatto M, Maria MC, et al. Accelerated aging effects on carbon fiber/epoxy composites. Compos Part B Eng 2017;110:298–306.

[6]   Grammatikos SA, Evernden M, Mitchels J, Zafari B, Mottram JT, Papanicolaou GC. On the response to hygrothermal aging of pultruded FRPs used in the civil engineering sector. Mater Des 2016;96:283–95. doi:10.1016/j.matdes.2016.02.026.

[7]   Korkees F, Arnold C, Alston S. Water Absorption and Low-Energy impact and Their Role in the Failure of ±45° Carbon Fibre Composites. Polym Compos 2018:1–12. doi:10.1002/pc.24269.

[8]   Kim H, Takemura K. Influence of water absorption on creep behaviour of carbon fiber/epoxy laminates. Procedia Eng 2011;10:2731–6. doi:10.1016/j.proeng.2011.04.455.

[9]   Pérez-Pacheco E, Cauich-Cupul JI, Valadez-González A, Herrera-Franco PJ. Effect of moisture absorption on the mechanical behavior of carbon fiber/epoxy matrix composites. J Mater Sci 2013;48:1873–82.

[10]   Saito H, Kimpara I. Damage evolution behavior of CFRP laminates under post-impact fatigue with water absorption environment. Compos Sci Technol 2009;69:847–55. doi:10.1016/j.compscitech.2008.03.025.

[11]   Kafodya I, Xian G, Li H. Durability study of pultruded CFRP plates immersed in water and seawater under sustained bending: Water uptake and effects on the mechanical properties. Compos Part B Eng 2015;70:138–48. doi:10.1016/j.compositesb.2014.10.034.

[12]   Selzer R. Mechanical properties and failure behaviour of carbon fibre-reinforced polymer composites under the influence of moisture 1997:595–604.

[13]   Zafar A, Bertocco F, Rauhe JC. Investigation of the long term effects of moisture on carbon fibre and epoxy matrix composites. Compos Sci Technol 2012;72:656–66. doi:10.1016/j.compscitech.2012.01.010.

[14]   Vasiliev V V, Morozov E V. Advanced Mechanics of Composite Materials. vol. 53. 2nd ed. Oxford: Elsevier; 2007.

[15]   Ray BC. Temperature effect during humid ageing on interfaces of glass and carbon fibers reinforced epoxy composites. J Colloid Interface Sci 2006;298:111–7. doi:10.1016/j.jcis.2005.12.023.

[16]   Dao B, Hodgkin J, Krstina J, Mardel J, Tian W. Accelerated aging versus realistic aging in aerospace composite materials. V. The effects of hot/wet aging in a structural epoxy composite. J Appl Polym Sci 2010;115:901–10.

[17]   Costa ML, Rezende MC, de Almeida SFM. Effect of void content on the moisture absorption in polymeric composites. Polym - Plast Technol Eng 2006;45:691–8. doi:10.1080/03602550600609549.

[18]   Zafar A, Bertocco F, Schjødt-Thomsen J, Rauhe JC. Investigation of the long term effects of moisture on carbon fibre and epoxy matrix composites. Compos Sci Technol 2012;72:656–66.

[19]   Sethi S, Ray BC. Environmental effects on fibre reinforced polymeric composites: Evolving reasons and remarks on interfacial strength and stability. Adv Colloid Interface Sci 2015;217:43–67. doi:10.1016/j.cis.2014.12.005.

[20]   Almeida JHS, Souza SDB, Botelho EC, Amico SC. Carbon fiber-reinforced epoxy filament-wound composite laminates exposed to hygrothermal conditioning. J Mater Sci 2016;51:1–12. doi:10.1007/s10853-016-9787-9.

[21] Cheng X, Baig Y, Li Z. Effects of hygrothermal environmental conditions on compressive strength of CFRP stitched laminates. J Reinf Plast Compos 2011;30:110–22. doi:10.1177/0731684410384894.

[22] Kawai M, Yagihashi Y, Hoshi H, Iwahori Y. Anisomorphic constant fatigue life diagrams for quasi-isotropic woven fabric carbon/epoxy laminates under different hygro-thermal environments. Adv Compos Mater 2013;22:79–98. doi:10.1080/09243046.2013.777172.

[23] ASTM D3171. Standard Test Methods for Constituent Content of Composite Materials. Am Soc Test Mater 2015.

[24] ASTM D 5229. Standard Test Method for Moisture Absorption Properties and Equilibrium Conditioning of Polymer Matrix Composite Materials. Am Soc Test Mater 2014.

[25] ASTM D 6641. Standard Test Method for Compressive Properties of Polymer Matrix Composite Materials Using a Combined Loading Compression (CLC) Test Fixture. Am Soc Test Mater 2009.

[26] ASTM D2344. Standard Test Method for Short-Beam Strength of Polymer Matrix Composite Materials and Their Laminates. Am Soc Test Mater 2016.

[27] Campbell FC. Manufacturing Processes for Advanced Composites. Oxford: Elsevier Advanced Technology; 2004.

[28] ASTM D7136. Standard Test Method for Measuring the Damage Resistance of a Fiber-Reinforced Polymer Matrix Composite to a Drop-Weight Impact Event. Am Soc Test Mater 2015.

[29] Zhang D, Heider D, Jr JWG. Void reduction of high-performance thermoplastic composites via oven vacuum bag processing. J Compos Mater 2017;51:4219–30. doi:10.1177/0021998317700700.

[30] Choi HS, Ahn KJ, Nam J, Chun HJ. Hygroscopic aspects of epoxy / carbon fiber composite laminates in aircraft environments. Compos Part A Appl Sci Manuf 2001;32:709–20.

[31] Vanlandingham MR, Eduljee RF, Gillespie JW. Moisture Diffusion in Epoxy Systems 1998:787–98.

[32] Torres A, Abad MJ, Cano J, Lo J, Lo I, Nogueira P, et al. Effect of Water Sorption on the Structure and Mechanical Properties of an Epoxy Resin System. J Appl Polym Sci 2000;80:71–80.

[33] Li Y, Cordovez M, Karbhari VM. Dielectric and mechanical characterization of processing and moisture uptake effects in E-glass / epoxy composites 2003;34:383–90.

[34] Martin K. Analysis of Failure in Fibre Polymer Laminates The theory of Alfred Puck. New York: Springer; 2008.

[35] Ma L, Meng L, Fan D, He J, Yu J, Qi M, et al. Interfacial enhancement of carbon fiber composites by generation 1-3 dendritic hexamethylenetetramine functionalization. Appl Surf Sci 2014;296:61–8. doi:10.1016/j.apsusc.2014.01.039.

[36] Gao SL, Mäder E, Zhandarov SF. Carbon fibers and composites with epoxy resins: Topography, fractography and interphases. Carbon N Y 2004;42:515–29.

doi:10.1016/j.carbon.2003.12.085.

[37]   Agarwal BD, Broutman LJ, Chandrashekhara K. Analysis and Performance of Fibre Composites. 3rd ed. John Wiley & Sons, Inc; 2006.

[38]   Hunkley JA, Connell JW. Resin Systems and Chemistry: Degradation Mechanisms and Durability. In: Pochiraju K V, Tandon G, Schoeppner GA, editors. Long-Term Durab. Polym. Matrix Compos., 2012.